https://dx.doi.org/10.1016/j.jclepro.2023.137413

Aerodynamic performance improvements for a Savonius turbine above a forward-facing step via inclined solar panel: a computational study

Haoyang Lu[a]; Lei Zhou[c,*]; Jiahao Wen[b]; Hui Tang[d]; Peng Guo[b]; Tim K.T. Tse[c]; Hongfu Zhang[b,*]

[a] School of Civil Engineering, Harbin Institute of Technology, Harbin 150090, China

[b] School of Civil Engineering, Northeast Forestry University, Harbin, 150040, China

[c] Department of Civil and Environmental Engineering, The Hong Kong University of Science and Technology, Clear Water Bay, Kowloon, Hong Kong, China

[d] Department of Mechanical Engineering, The Hong Kong Polytechnic University, Kowloon, Hong Kong, China

*Corresponding Author: Lei Zhou; Hongfu Zhang

E-mail addresses: lzhouau@connect.ust.hk (Lei Zhou); zhanghongfu@nefu.edu.cn (Hongfu Zhang)

Abstract

The transformation of urban energy structure is an urgent problem to be solved in sustainable construction. To fully exploit and utilise renewable energy, this study proposes a novel wind–solar energy hybrid harvesting system that combines an inclined solar panel and a Savonius wind turbine installed on a building roof. The effects of the tilt angle of the solar panels and tip speed ratios (TSRs) on the aerodynamic performance of the turbine were investigated using high-fidelity large-eddy simulations (LES) at a Reynolds number of $Re = 4.45 \times 10^5$. Five tilt angles in the range of 30° to 60° were tested, and the range of TSR was 0.2 to 1.6. For comparison, two other installation cases were also studied, including the case of a Savonius turbine alone and

the case of a single Savonius turbine placed at a fixed height position on a forward-facing step. The results showed that the power coefficient of the Savonius turbine increased and then decreased with tilt angle or TSR. When TSR = 1, the power coefficient in the system reached a maximum value of C_{pmax} = 0.638 at a tilt angle of 45°, 254.4% and 11.7% higher than those of the other two installation cases, respectively. The flow-field comparison results reveal why the proposed system can improve the energy harvesting efficiency. The presence of a solar panel with a suitable tilt angle increases the velocity and volume of the airflow hitting the advancing blade, creating a greater pressure difference around the blades that is caused mainly by the decrease in the low pressure on the concave surface of the advancing blade. Thus, the net torque applied to the turbine blades increases, which is conducive to driving turbine rotation. The proposed system is beneficial for improving the aerodynamic performance of Savonius turbines and the utilisation of renewable energy in urban areas.

Keywords: Aerodynamics; Large-eddy simulations; Savonius wind turbine; Solar panel; Urban wind energy

1. Introduction

With the intensification of the energy crisis and global warming, the development and utilisation of renewable energy have attracted great interests [1-5]. Wind and solar energy are widely used as clean and sustainable energy sources in offshore, urban, and mountainous areas.[6-9]. Energy projects in urban environments are close to end-users, reducing costs and avoiding transmission power losses [10].

Wind energy in a city can be captured using small-scale turbines [11]. Depending on the direction of the axis of rotation, wind turbines can be classified as horizontal-axis wind turbines (HAWTs) or vertical-axis wind turbines (VAWTs) [12-15]. Compared with HAWTs, VAWTs do not need to be aligned with the incoming wind, and have low noise levels, low maintenance costs, and the ability to operate in highly turbulent wind conditions. As such, they are more suitable for utilisation in urban built environments[16]. Previous studies

have found that the location of VAWTs on the roof has a significant effect on the power-generating efficiency [17, 18]. Liu et al. [19] compared the difference in the power coefficients of VAWTs under different installation cases. The results showed that the power coefficient of a wind turbine placed on a step with a fixed height was higher than that of a wind turbine placed on a flat surface for both a single wind turbine and three wind turbines in a fixed arrangement. Larin et al. [20] studied the effects of the placement position, blade number, and circumferential length on the turbine power for two types of VAWTs placed on the roof of a building. The results showed that the power coefficient increased from 0.043 to 0.24 in the optimal case of a seven-bladed turbine with double-cut blades installed on the roof of a building.

The Savonius wind turbine is one of the simplest VAWTs. It consists of two semi-circular blades facing opposite directions, with a small overlap between the blades and an overall s-shaped cross-section. The rotor is not only simple and robust in construction but also has good self-starting properties and can operate at low cut-in wind speeds [21, 22]. Unfortunately, its energy conversion efficiency is low; its aerodynamic performance must be improved. Research has been conducted to make it an effective design for urban energy harvesting, including blade shape improvement, adding deflectors, and layout optimisation [23-27]. Aboujaoude et al. [28] added an axisymmetric truncated cone deflector around the Savonius turbine to investigate its effect on increasing turbine power. Three-dimensional numerical simulations showed that the axisymmetric deflector improved the turbine power by 25% in all wind directions, and the maximum power coefficient reached C_{pmax} = 0.31. Talukdar et al. [29] experimentally investigated the effect of a new arc-elliptical-bladed rotor on the performance improvement of Savonius turbines compared with the conventional semi-circular-bladed rotor. They found that the power coefficient was increased from 0.176 to 0.213 with the assistance of arc-elliptical blades. To improve the performance of the Savonius turbine, Mohamed et al. [30] introduced an obstacle plate placed at the windward side of the Savonius turbine and optimised the shape of the blade skeleton. The CFD simulation results indicated at least a 30% increase in the power coefficient in

67 the simulated range of the tip speed ratio ($0.3 \leq TSR \leq 1.4$). Golecha et al. [31] used a deflector plate to
68 improve the performance of the Savonius rotor by providing a flow obstacle to the returning blade. The results
69 showed that incorporation of the optimally positioned deflector plate resulted in a 50% power coefficient
70 increase in the Savonius rotor at TSR = 0.82.

71 Although many measures have been demonstrated to improve turbine performance, some simple devices
72 (e.g. deflector plates) are more beneficial for maintaining the simplicity, compactness, robustness, and low
73 cost of Savonius turbines, and bring efficiency improvements at lower cost and with less complexity [32].

74 Solar panels are thin-plate structures with simple aerodynamic shapes and are widely used to collect solar
75 energy. They are suitable for placement on the roof of a building to facilitate energy harvesting [33]. The
76 presence of solar panels has a significant impact on the flow-field of a roof [34].

77 Accordingly, we propose a novel wind–solar energy hybrid energy harvesting system in which wind
78 turbines and solar panels are combined and placed on a building roof. The system is feasible and
79 environmentally friendly; its working principle is shown in Fig. 1. In this system, the solar panel is used as a
80 deflector plate. The solar panel and the building roof work in synergy to enhance the performance of the wind
81 turbine more effectively, thereby increasing wind energy utilisation. Moreover, the system allows for the
82 simultaneous collection of two kinds of clean energy. Wind and solar energy complement each other because
83 wind speed and solar irradiation vary with daily solar cycles and seasons, which creates a more stable power
84 generation system.

85 In this study, the performance of a Savonius turbine in the system was tested at different tilt angles and
86 TSRs. For comparison, two baseline cases were chosen: one with a Savonius turbine alone and one with a
87 single Savonius turbine placed at a fixed height on a forward-facing step to simulate roof conditions. The main
88 research includes the following: (1) The effect of different tilt angles of the solar panel on the power coefficient
89 and flow-field of the Savonius turbine was studied to determine the optimal angle. (2) The aerodynamic

performance of the Savonius turbine in the hybrid harvesting system with an optimal angle at different TSRs was investigated and compared with two base cases to test the effect of the hybrid system in improving wind energy utilisation. Finally, we briefly estimate the CO2 emissions that could be reduced by utilising a Savonius wind turbine to generate electricity in the novel hybrid powertrain.

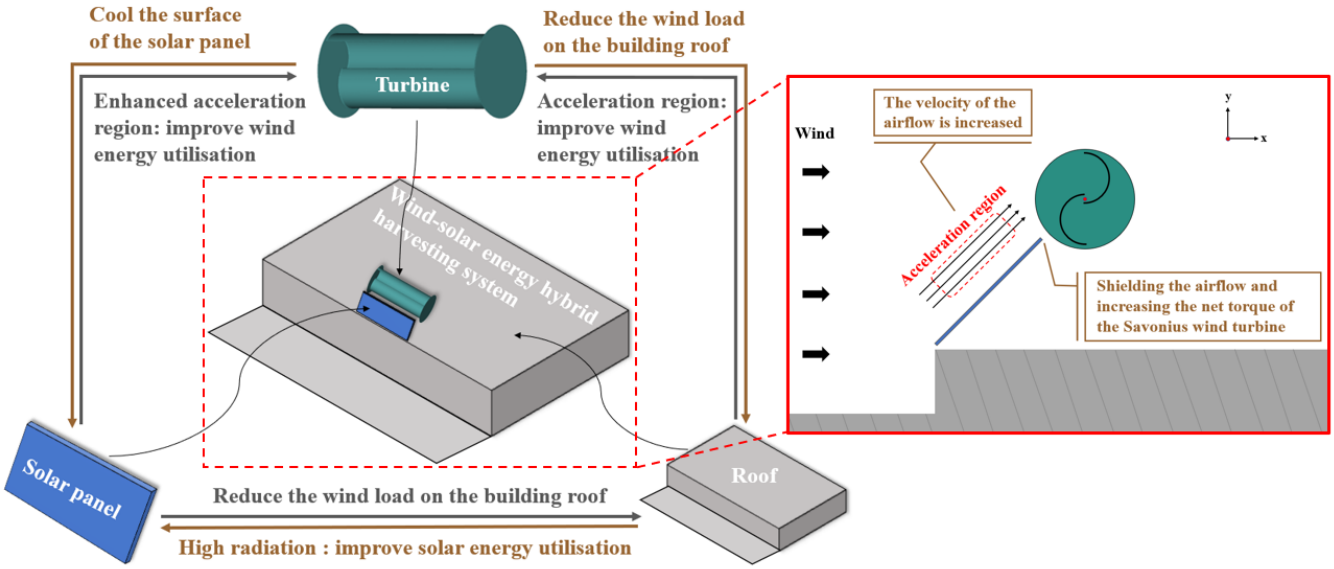

Fig. 1. Working principle of wind–solar energy hybrid harvesting system.

2. Numerical method

Regarding the VAWT calculation, the relevant physical effects can be captured, and the numerical computation cost can be reduced using two-dimensional models. However, the estimation of the power coefficient is not sufficiently reliable [35]. Ferrari et al. [36] reported that the power coefficient calculated by two-dimensional numerical simulations is often overestimated and the shape of the characteristic curve cannot be accurately replicated; the same conclusion was obtained by Li et al. [37]. A power coefficient using three-dimensional models has higher accuracy, and can more reasonably estimate the performance of a VAWT. Thus, a high-fidelity three-dimensional numerical simulation was used in this study for the Savonius wind turbine.

2.1 Savonius geometry

The installation schematic of the Savonius wind turbine is shown in Fig. 2. A forward-facing step was used to simulate the roof of the building. The step height H was set to 6 m, the height of a typical small building. The horizontal distance from the centre of the Savonius wind turbine to the front of the step is X, and the vertical distance to the surface of the step is Y. For all investigated cases, X and Y were fixed, and both equal to 1.5 m. There are typically one to three semi-cylindrical blades in a conventional Savonius wind turbine. Based on existing research results, we selected a two-blade system with the best performance [21]. The overall diameter of the Savonius rotor (D) was set to 1 m; the main blade diameter (D_b) was 0.93 m, and the overall length (L) was 2 m. The ratio of the turbine length to turbine diameter (L/D_b) is referred to as the aspect ratio (AR), and was 2.15. The semi-cylindrical blade diameter (d) was 0.5 m; the overlap distance (e) was 0.075 m, and the thickness of all blades (t) was set to 4 mm. The ratio e/d represents the dimensionless gap width. Fujisawa [38] and Akwa et al. [21] proposed that the optimal turbine efficiency was generated at $e/d = 0.15$. Thus, the overlap ratio in this study was set as 0.15. The length (L_p) of the solar panel was 2 m; the width (W_p) was 1.5 m, and the thickness (t_p) was 0.03 m. The tilt angle of the solar panel is denoted as α.

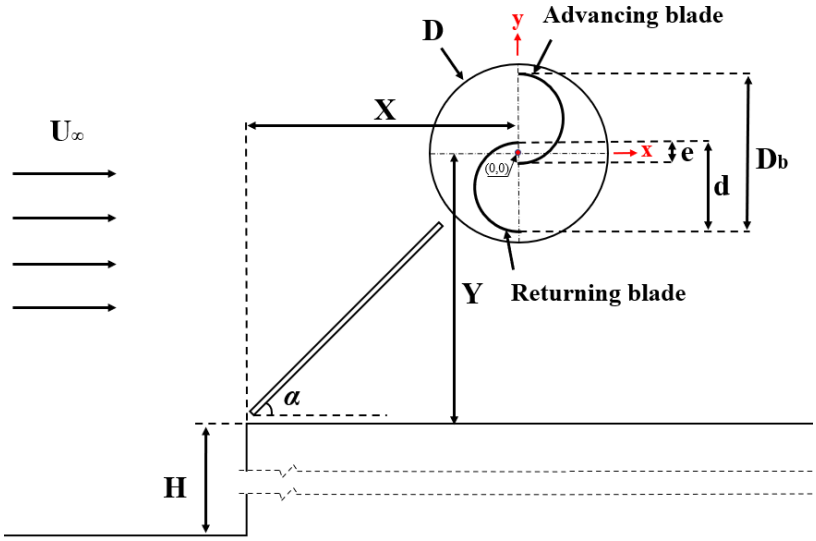

Fig. 2. Schematic of Savonius turbine viewed from positive z-axis.

2.2. Computational domain and boundary conditions

The computational domain and boundary conditions are illustrated in Fig. 3. The computational domain was set to 70 m (70*D*), 30 m (30*D*), and 30 m (30*D*) along the x-, y-, and z-directions, respectively. In the x-direction, the lengths ahead and behind the step were set to 30 m (30*D*) upstream and 40 m (30*D*) downstream, respectively. The entire computational domain was divided into three parts from the inside to the outside: the rotating, wake, and stationary regions. The rotating region indicates the flow-field near the Savonius turbine surfaces; its diameter and length were set to 1.1 *D* and 1.1 *L*. Outside the rotation region is the wake region, where the grid was refined to ensure calculation accuracy [19, 39]. For numerical computation of the unsteady region, a sliding mesh was applied in the rotating region with varying angular speeds according to the TSR. The data of the rotating and static regions were transmitted through the mesh interface zone in the shared faces where the meshes overlapped [40]. The outermost stationary region represents the majority of surrounding air.

For the boundary conditions, a no-slip condition was applied to the fixed walls of the stationary domain, as well as on the solar panel and wind turbine. A constant velocity of 7 m/s with a turbulence intensity of 5% was imposed at the inlet of the computational domain, and a pressure outlet condition (uniform and constant atmospheric pressure) with zero gradient for the velocity and turbulence quantities was imposed at the outlet. Both sides and the top surface of the domain were set as symmetry boundary conditions.

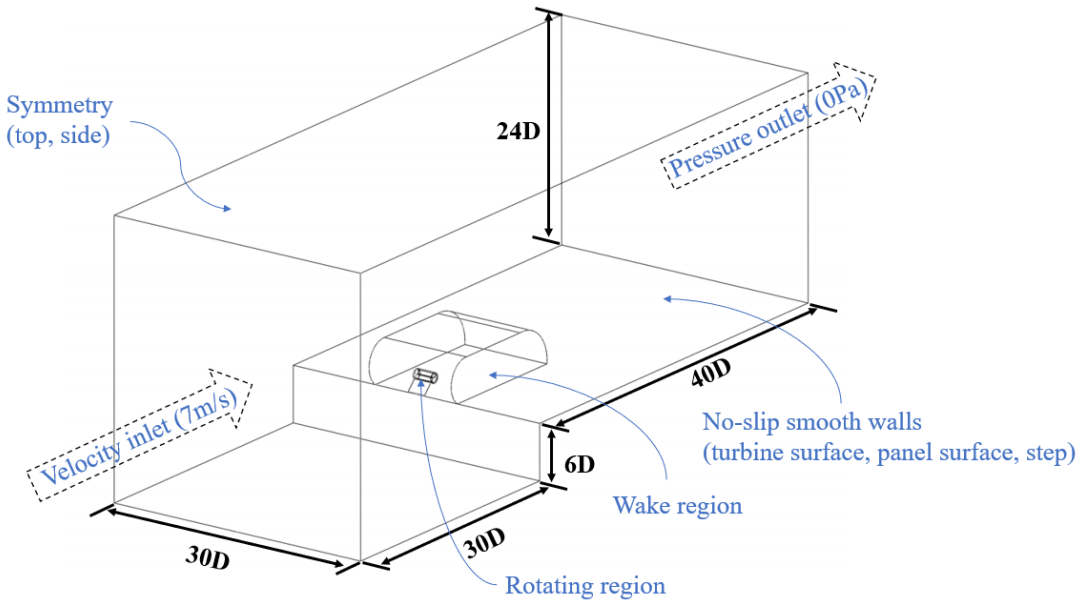

Fig. 3. Computational domain and boundary conditions of a solar panel and a Savonius wind turbine placed on a forward step at a fixed height.

2.3. Mesh generation

The grids used for the calculations in this study consisted of unstructured tetrahedral elements, as shown in Figs. 4 and 5. An appropriate magnification was used from the inside to the outside of the grid such that the number of grids could be reasonably reduced to improve the calculation efficiency while ensuring accuracy. As small flow structures are typically produced close to solid walls, a finer mesh adjacent to solid walls is crucial. Thus, the inflation option was introduced, with a boundary layer mesh of five inflation layers and a growth rate of 1.1 applied to the blade and solar panel surfaces. The first grid height of the boundary layer was 0.00015 m to satisfy the requirements of the turbulence model. The grid near the solar panel and step was refined to capture the flow-field details.

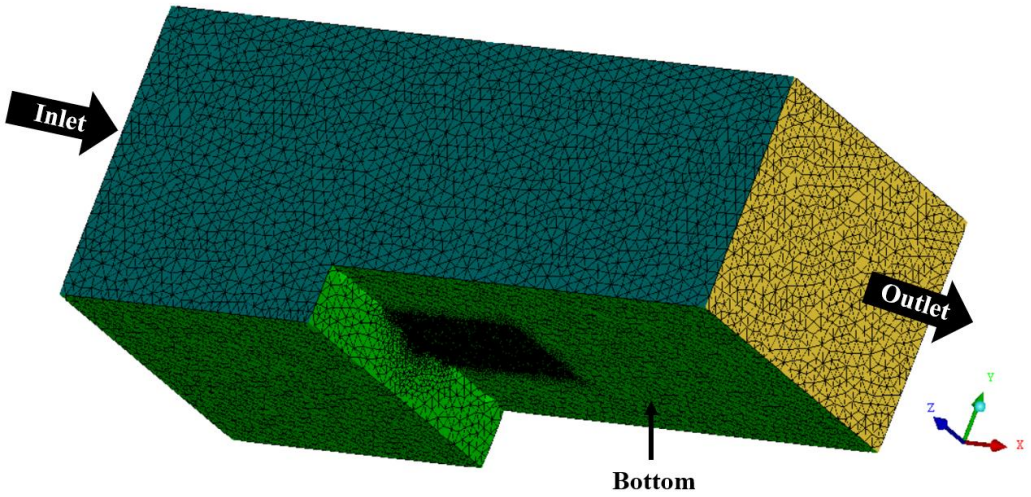

Fig. 4. Global grid, generally showing the underside of the domain from the outlet.

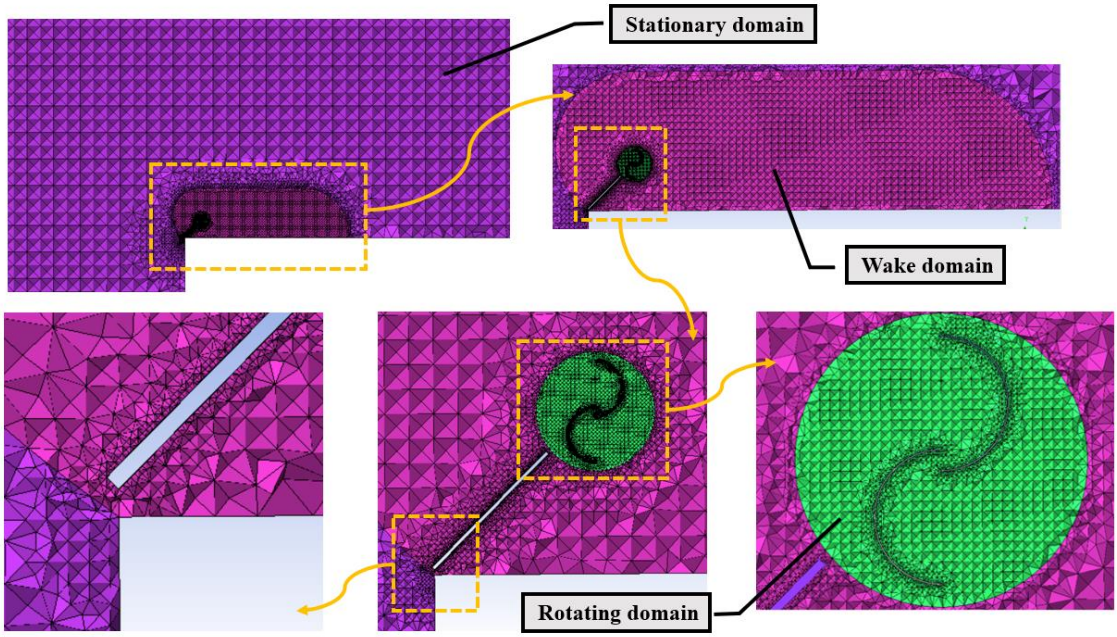

Fig. 5. Side view of computational domain with different zone grid densities.

2.4. Simulation setup

The segregated approach was selected to solve the discretised continuity and momentum equations, and a second-order implicit formula was used for temporal discretisation. The SIMPLE algorithm was adopted in the simulation to solve the pressure–velocity coupling problem. A bounded central difference scheme was adopted for the spatial discretisation of the momentum.

Twenty iterations were performed at each time step to ensure that the residual was sufficiently small, which was set to 10^{-5}. Considering the calculation accuracy and efficiency comprehensively, the time step was set to 0.001 s, which is more refined than the setting of 1/120 cycles (0.0035 s when TSR = 1 in this study) [39].

An LES has a lower time and computational cost than direct numerical simulation (DNS) and higher information integrity than Reynolds-averaged Navier–Stokes (RANS). Li et al. [37] reported that the LES results are in better agreement with experiments than RANS results when investigating the aerodynamic characteristics of VAWTs. Thus, at the Reynolds number $Re = 4.45\times10^5$, LES based on the Smagorinsky-Lilly model was chosen for the numerical calculation [40]. A typical y+ plot obtained through post-processing

is shown in Fig. 6, and satisfies the calculation requirements of y+ <5.

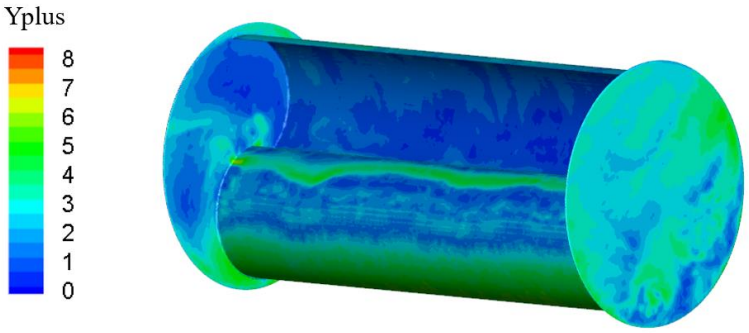

Fig. 6. Plots of simulation results of typical y+ values for a Savonius wind turbine mounted on a forward-facing step with incoming wind speed U_∞ = 7 m/s and TSR = 1.

2.5. Case summary

This study includes two baseline cases: the first with a Savonius turbine alone (ST) and the second with a single Savonius turbine placed at a fixed height on a forward-facing step (ST-ffs).

For the wind–solar energy hybrid harvesting system (combination of Savonius wind turbines and a solar panel mounted on a forward-facing step, abbreviated as ST-sp-ffs), simulations were first performed at TSR = 1, and the solar panel was placed at various tilt angles (α = 30°, 40°, 45°, 50°, and 60°). The selection of the tilt angle studied is based on the range of tilt angles commonly used for solar panels in China, and the need to achieve a desirable deflective effect in the flow field structure. Then, the tilt angle case with the highest power coefficient was selected for the numerical simulation with different TSRs (0.2, 0.4, 0.6, 0.8, 1.2, 1.4, 1.5, 1.6). The simulated cases are summarized in Table 1.

Table 1 Working case settings

Installation case	Tilt angle α (°)	Tip speed ratio TSR	Place position X/W_p
ST (A Savonius turbine alone)	-	0.2, 0.4, 0.6, 0.8, 1.2, 1.4	-
ST-ffs	-	0.2, 0.4, 0.6, 0.8, 1.2, 1.4, 1.5, 1.6	-

(A Savonius turbine on a step)			
ST-sp-ffs (Combination of Savonius wind turbine and solar panel on a step, namely the wind–solar energy hybrid harvesting system)	30	1	1
	40	1	1
	45	0.2, 0.4, 0.6, 0.8, 1.2, 1.4, 1.5, 1.6	1
	45	1	1, 1.2
	50	1	1, 1.2
	60	1	1

3. Simulation results validation

3.1. Data processing

To measure the ability of a wind turbine to convert wind energy into mechanical energy, two important parameters, the torque coefficient C_t and power coefficient C_p [19, 24, 41], are introduced in this study. They are expressed as

$$C_p = \frac{Power\ output\ from\ the\ turbine}{Available\ power\ in\ the\ incoming\ wind} = \frac{T \times \omega}{\frac{1}{2}\rho A U_\infty^3}$$

where T is the torque developed around the axis of the wind turbine ($N{\cdot}m$), ω is the angular velocity of the turbine (rad/sec), ρ is the air density (kg/m^3), A is the projected area of the turbine (m^2), and U_∞ is the incoming wind speed.

$$C_t = \frac{actual\ torque\ generated\ by\ the\ turbine}{theoretial\ torque\ available\ in\ the\ incoming\ wind} = \frac{T}{\frac{1}{2}\rho A U_\infty^2 R}$$

where R is the radius of the turbine (m).

The tip speed ratio (TSR or λ) is defined as the ratio between the tangential speed of the blade tip and the incoming wind speed, and is calculated as

$$\lambda = \frac{\omega \times R}{U_\infty}$$

Thus, the relationship between C_p and C_t can be expressed as

$$C_p = C_t \times \lambda$$

3.2. Grid independence verification

The case of the hybrid system with $\alpha = 30°$ was used for grid-independence verification. The verification was performed by evaluating the C_p of turbine for grid densities of 4.5 million, 5.9 million, 7.4 million, and 10 million elements. The results are presented in Table 2. It is observed that C_p changes slightly from Refinement level 3. Considering the balance between accuracy and time cost, a grid of 7.4 million elements was chosen for subsequent numerical simulations.

Table 2 Grid-independence test at TSR = 1

Refinement level	Number of elements	C_t	C_p
1	4168168	0.341	0.341
2	5955438	0.278	0.278
3	7328694	0.224	0.224
4	10751196	0.214	0.214

3.3. Model feasibility validation

Power coefficient C_p, a key indicator of wind turbine performance, is commonly used to verify the reliability of numerical results. The feasibility of the proposed numerical model under the grid parameters of this study was validated before proceeding to subsequent studies. First, the case of a Savonius wind turbine alone was used for validation. For Savonius turbines with similar geometric parameters in this study, C_p was tested in particle image velocimetry experiments by Dobrev et al. [42]; later numerical simulations were conducted by Ferrari [36] and Longo [43]. The results are compared in Table 3; the error was within 8%.

Subsequently, the case of a Savonius turbine on a step was used for validation. As shown in Fig. 7, the C_p values at different TSRs are consistent with the results of Liu et al. [19] and Goh et al. [18]. Thus, it is believed that the reliability of the numerical simulation is acceptable for subsequent simulation processes.

Table 3 Feasibility verification of numerical model for the case of a Savonius turbine alone

Data source	Method	C_p (Error%)		
		TSR = 0.6	TSR = 0.8	TSR = 1
Current study	Numerical simulation	0.178	0.186	0.180
Dobrev [42]	PIV experiment	0.176 (1.14%)	0.180 (3.33%)	0.167 (7.78%)
Ferrari [36]	Numerical simulation	0.186 (4.3%)	0.202 (7.92%)	0.188 (4.26%)
Longo [43]	Numerical simulation	0.186 (4.3%)	0.201 (7.46%)	0.187 (3.74%)

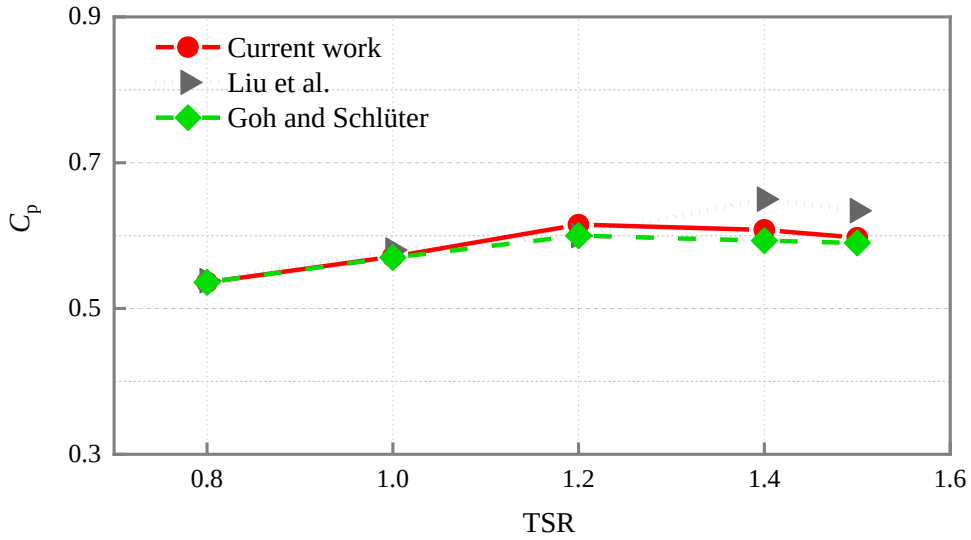

Fig. 7. Comparison of C_p curves for a single Savonius turbine placed on a forward-facing step.

4. Results and discussion

4.1. Aerodynamic performance of Savonius turbine

C_t and C_p were analysed as measures of Savonius turbine performance. The C_p values at selected tilt angles ($\alpha = 30°, 40°, 45°, 50°, 60°$) in the hybrid system at TSR = 1 are shown in Fig. 8; the C_p values for the two base cases are indicated by coloured dotted lines. It is observed that the C_p values of the Savonius turbine in the hybrid system exceed those of the Savonius turbine alone at most tilt angles and those of a Savonius turbine on a step in an angle range of approximately 40–45°. The C_p value of the Savonius turbine reached the

maximum (C_{pmax} = 0.638) for all tested angles at α = 45°, with a power increase of approximately 254.4% compared to a Savonius turbine alone ($C_{p,\,ST}$ = 0.180) and 11.7% compared to a Savonius turbine on a step ($C_{p,\,ST\text{-}ffs}$ = 0.571). When the tilt angle was approximately 60°, the Savonius turbine failed owing to inappropriate airflow guidance. The tilt angle of the solar panel in the hybrid system has a significant impact on the performance of the Savonius turbine; a reasonable tilt angle is essential for improving energy efficiency.

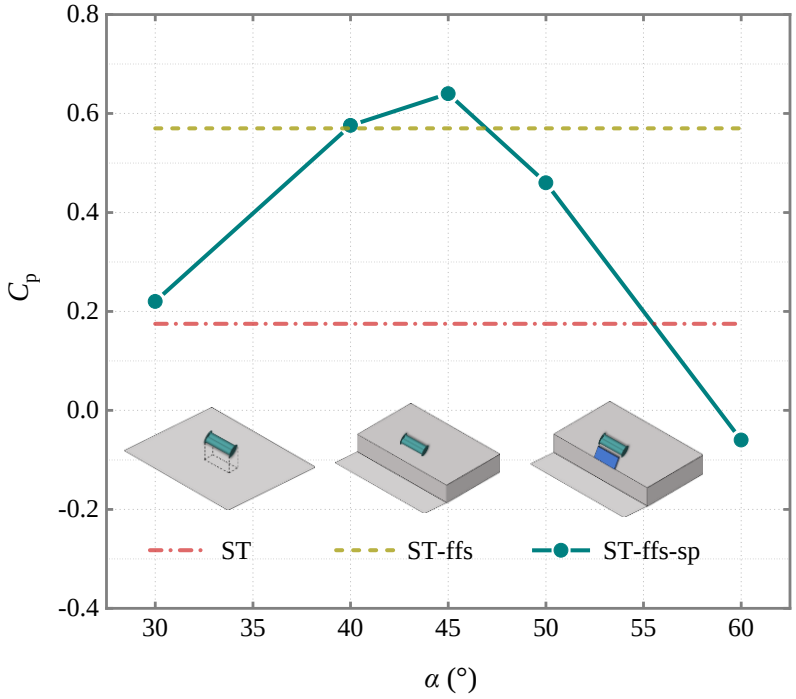

Fig. 8. Comparison of C_p curves with different tilt angles (α).

Fig. 9 compares the instantaneous C_t in the hybrid system with typical tilt angles and the instantaneous C_t for a Savonius turbine on a step. It is observed that a solar panel at α = 45° significantly enhances C_t, producing the highest peak value compared to all the cases. However, with tilt angles of 30° and 60°, C_t was reduced with the presence of the solar panel, especially at 60°. As the parameter settings of the numerical simulation such as inlet wind speed and TSR are consistent for all cases in Fig. 9, the variation in C_t can indicate the variation in C_p.

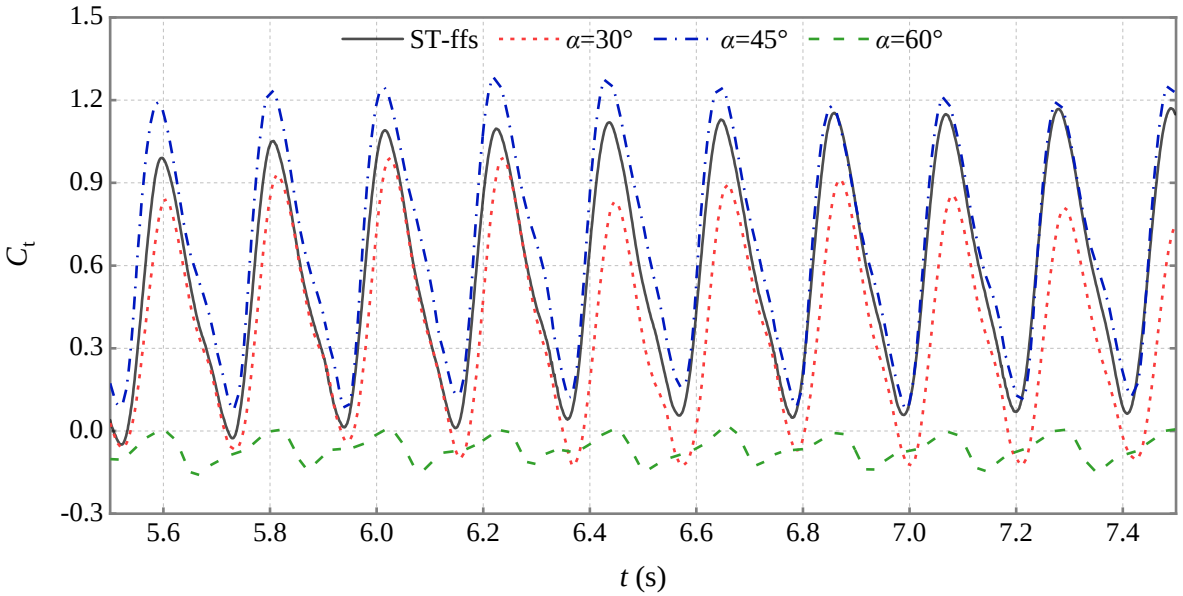

Fig. 9. Instantaneous values of C_t with different tilt angles (α).

Previous results have shown that Savonius turbine performance is optimal at $\alpha = 45°$. Thus, we performed simulations for the hybrid system with α = 45° at other TSRs (0.2–1.6); the results are presented in Fig. 10. The C_p results for the two baseline cases and another study are also included in Fig. 10, as well as the existing result from another study[18]. It is observed that C_p in the hybrid system with $\alpha = 45°$ at the tested TSRs is significantly higher than C_p for a Savonius turbine alone and for a Savonius turbine on a step at approximately TSR < 1.2. C_p increases to the maximum value with an increase in TSR and then decreases with a further increase in TSR. The peak C_p of Savonius wind turbines occurs at different TSRs in different installation environments. $C_{pmax} = 0.638$ occurs at TSR = 1 for the hybrid system with $\alpha = 45°$; $C_{p(max,ST)} = 0.187$ occurs at TSR = 0.8 for a Savonius turbine alone, and $C_{p(max,ST\text{-}ffs)} = 0.615$ occurs at TSR = 1.2 for a Savonius turbine on a step. In all cases, the maximum power coefficient is observed at $\alpha = 45°$; C_{pmax} is 241.2% greater than $C_{p(max,ST)}$, and 3.7% greater than $C_{p(max,ST\text{-}ffs)}$. Thus, it is concluded that the power performance of the turbine can be enhanced by installing a solar panel at a suitable tilt angle, improving wind energy utilisation.

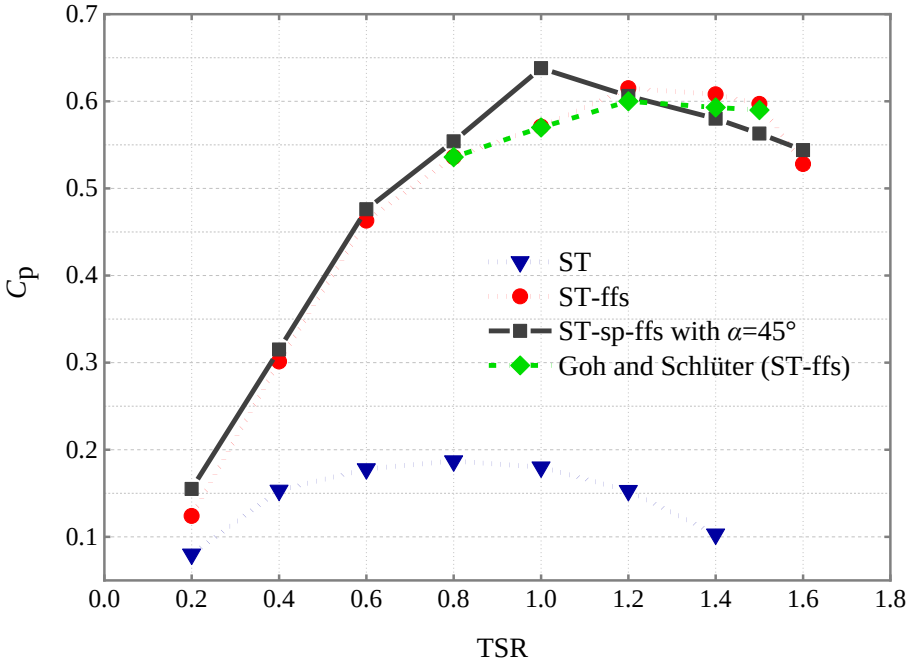

Fig. 10. Comparison of power coefficient in this study and Refs[18].

4.2. Flow-field of hybrid harvesting system

The power of the Savonius wind turbine is provided by the pressure difference on the blades, which can be interpreted as a difference in the drag force. To understand the interaction of forces or momentum between the blade surface and fluid flow, it is necessary to investigate the pressure distribution on the Savonius blade surface. To better represent the pressure difference, the normalised pressure can be calculated as

$$\frac{P}{q} = \frac{2P}{\rho U_\infty^2}$$

where P is the pressure, and $q = \frac{\rho U_\infty^2}{2} = 30$ (Pa) is the dynamic pressure.

The normalised pressure contours of the Savonius turbine on the step and the hybrid system with typical tilt angles are shown in Fig. 11. Relatively similar pressure distributions around the turbine blades are observed for the case of α = 45° and a Savonius turbine on a step (ST-ffs). Owing to the impulse of the airflow, positive pressure is generated on the concave surface of the advancing blade, while a negative pressure appears on the convex surface. Thus, there is a large pressure difference around the advancing blade. The additional force generated by the larger pressure difference leads to an increase in the net torque acting on the blade, resulting

in an increase in the C_p of the Savonius turbine, explaining the higher C_p in both cases. It is observed in Fig. 11(b) that the degree and range of high and low pressures on the blade surface at α = 30° are reduced; the reduction in the pressure difference of the advancing blade leads to relatively low power of the Savonius wind turbine. For the α = 60° case shown in Fig. 11(d), the tilt angle of the solar panel is too large, making it impossible for the airflow to hit the blade and generate a pressure difference to drive the turbine.

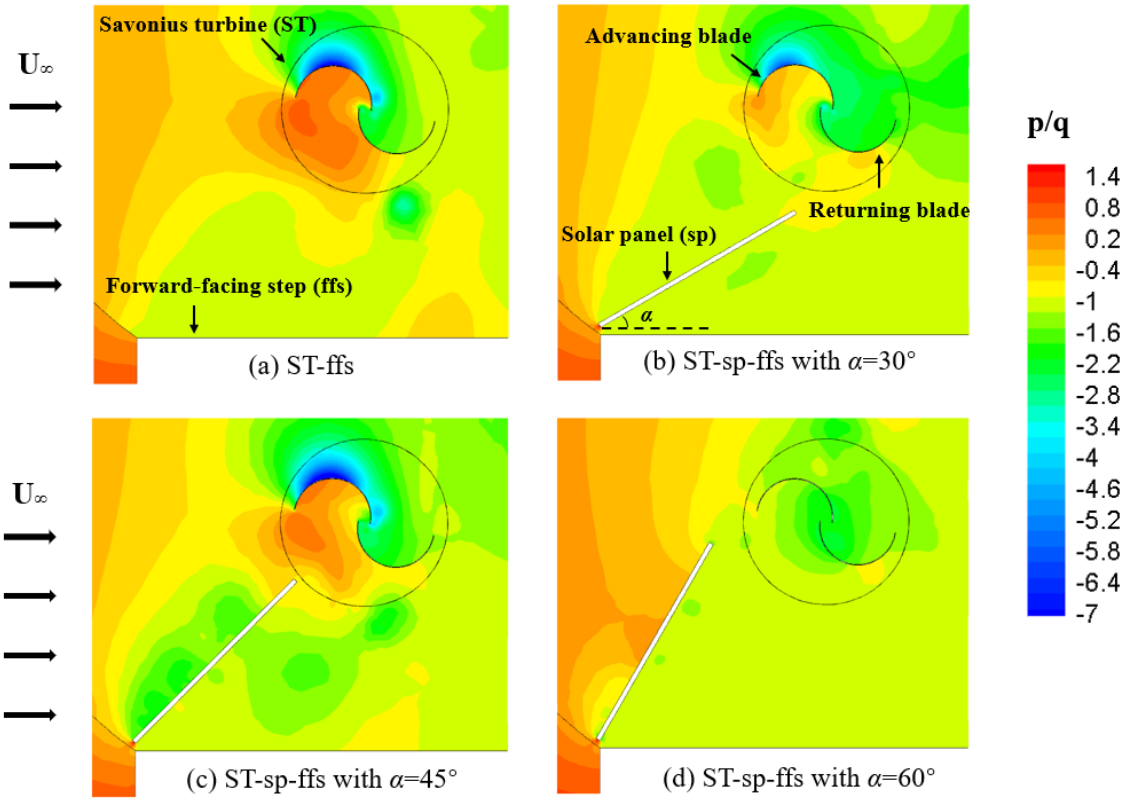

Fig. 11. Normalised pressure contours of ST-ffs and ST-sp-ffs with typical solar panel tilt angles at TSR = 1.

The pressure difference is presented in Fig. 13 to help analyse the pressure distribution along the blade surface for different cases. The data point locations are shown in Fig. 12. The driving on the advancing blade and the restriction on the returning blade were generated by the pressure difference between the upper and lower turbine surfaces. Comparing Fig. 13(a) and Fig. 13(c), the pressure distribution along the concave surfaces of the two blades differs slightly. For a solar panel with α = 45°, the low pressure on the convex surface of the advancing blade is smaller, resulting in a larger pressure difference, which is favourable for driving the advancing blade. The low pressure on the convex surface of the return blade is smaller and has a less restrictive effect on the return blade. For α = 30°, the pressure difference around the advancing blade was

significantly reduced, resulting in a decrease in C_p, as shown in Fig. 13(b). For $\alpha = 60°$, the pressure difference around the blade surface was essentially negligible, as shown in Fig. 13(d), and the Savonius wind turbine did not function. The highest C_p occurred at $\alpha = 45°$; the driving pressure difference of the advancing blade was the largest, and the restricting pressure difference of the returning blade was smaller.

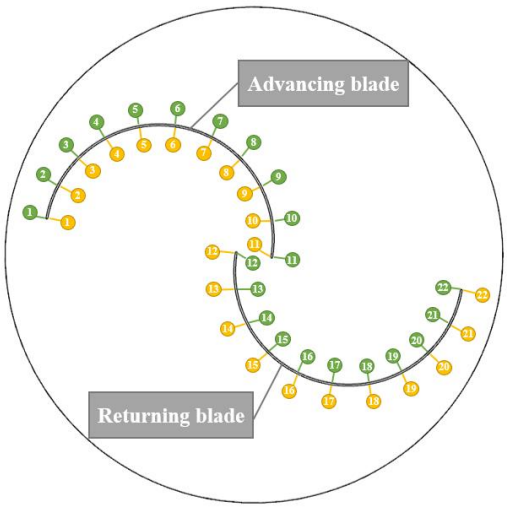

Fig. 12. Diagram of numbered positions.

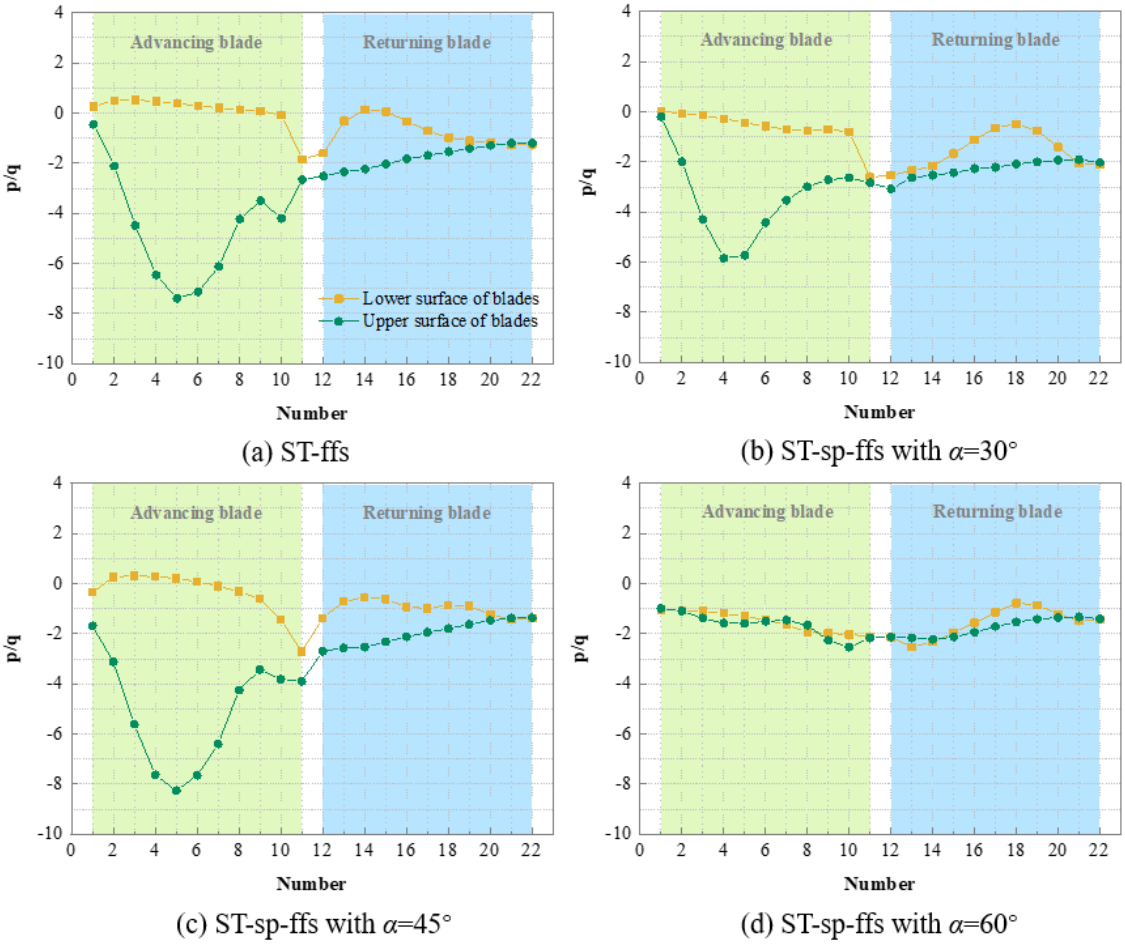

Fig. 13. Instantaneous normalised pressure distribution curves along blade surface at TSR = 1.

The velocity streamline plots of the Savonius turbine on the step and the hybrid system with typical tilt angles are shown in Fig. 14. It is observed that when the incoming wind approaches the step, it is influenced by the corner of the building and advances in the upwind direction along the step; flow separation occurs at the front boundary of the step[20, 44]. For the case without solar panels shown in Fig. 14(a), a large vortex was generated in front of the upper surface of the step, and an acceleration region was formed above the vortex. A small portion of the accelerated airflow moved along the passage between the vortex and the returning blade; the majority rushed to the blade, causing the turbine to rotate by striking the advancing blade. A similar streamline patterns can be found in the study of Liu et al. [19]. For the hybrid system, when the tilt angle is 30°, the solar panel disrupts the original vortex on the step and creates a large vortex above the panel surface, as shown in Fig. 14(b), causing the original acceleration region to shift upward, leading to a reduction in both the airflow and velocity toward the advancing blade. As shown in Fig. 14(d), the 60° tilt-angle solar panel guides most of the airflow away from the advancing blade, resulting in power failure of the Savonius turbine. For $\alpha = 45°$, as shown in Fig. 14(c), the solar panel played a positive role in guiding the airflow separated by the edge of the step, blocking part of the airflow originally flowing to the passage. As a result, the airflow velocity in the acceleration region is increased, allowing higher velocity airflow to hit the advancing blades, generating a greater wind load to drive the rotation of the wind turbine, thus improving its aerodynamic performance.

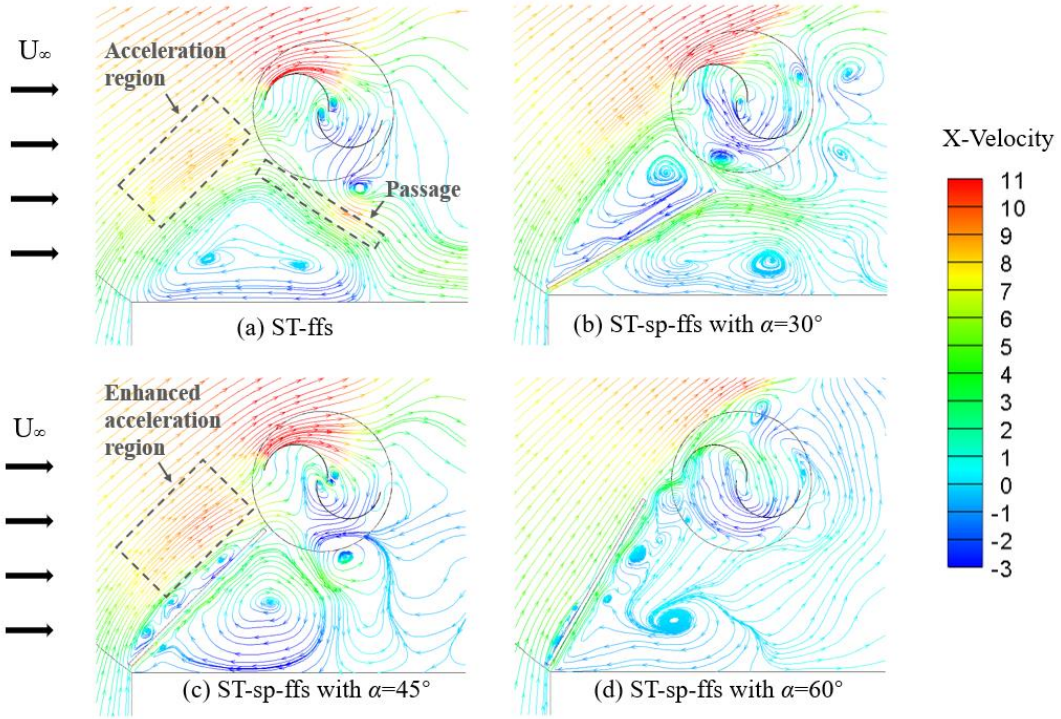

Fig. 14. Velocity streamline plots for ST-ffs and ST-sp-ffs with typical solar panel tilt angles at TSR = 1.

To investigate the reason for the highest C_p at α = 45°, the normalised pressure contours at different azimuth angles are shown in Fig. 15. For the case of a single Savonius turbine placed on a forward-facing step, as shown in Figure 15(b), the pressure distribution is similar to that of existing studies[18, 19]. In Fig. 15(b), when the tilt angle of the solar panel in the hybrid system is 45°, there is a more significant pressure difference on the advancing blade at all investigated azimuth angles, mainly caused by the larger area of the low-pressure region on the convex surface. The returning blade is less restricted due to the smaller high-pressure region on its convex surface (which is more pronounced at azimuths of 60° and 120°). A larger pressure difference indicates that the turbine is subjected to additional wind loading. As a result, in the α = 45° case, a higher net torque is produced for the Savonius turbine on a step, which leads to an increase in the C_p value.

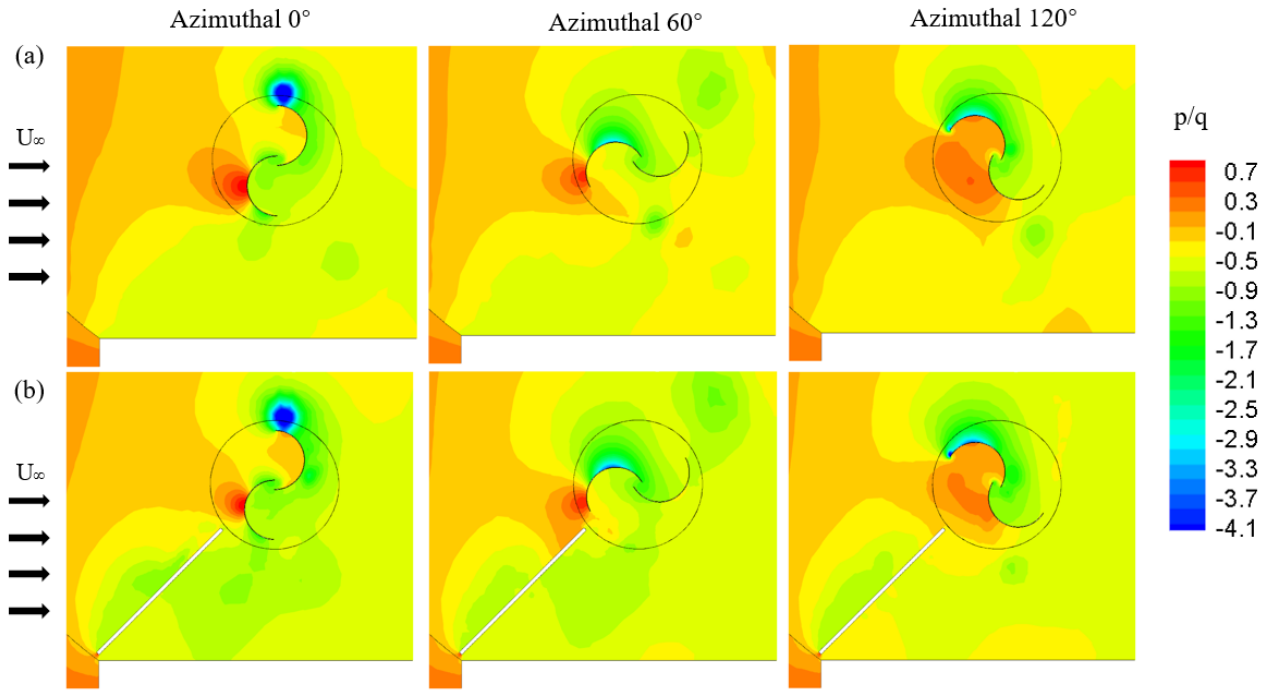

Fig. 15. Normalised pressure contours at different azimuth angles for (a) ST-ffs; (b) ST-sp-ffs with $\alpha = 45°$.

Figs. 17 and 18 show a comparison of the vertical profiles of the normalised streamwise velocity and turbulence intensity (TI), respectively, at TSR = 1 and at different positions (P1 to P5) shown in Fig. 16. The legend range is -1.5 < y/D < 0.5, where y/D = 0 is the height of the geometric centre on the Savonius turbine. As shown in Fig. 17, a solar panel with an extremely large tilt angle ($\alpha = 60°$) leads to a significant reduction in the velocity in the upper region of the panel, resulting in a loss of momentum. The $\alpha = 45°$ case has a higher velocity than all other cases in the region of a certain height on the panel. At positions P4 and P5, which are closer to the Savonius turbine, the region where the airflow can directly hit the advancing blade to drive the turbine rotation is defined as the "effective region". In the effective region, the $\alpha = 45°$ case has a higher velocity, implying better performance of the Savonius turbine. In contrast, for the $\alpha = 30°$ case, the velocity is lower than for the Savonius turbine on a step because the panel does not play a positive guiding role, leading to a lower C_p after installation of the solar panel. TI is calculated as U'/U_∞, where U' is the root mean square of the streamwise velocity. It is observed that TI tends to increase overall as the airflow develops from the edge of the step to the front of the Savonius turbine, as shown in Fig. 18. Addition of the solar panel leads to a significant increase in TI at a certain height on the upper surface of the panel, particularly in the $\alpha = 45°$ case,

where the maximum value of TI reaches 0.35.

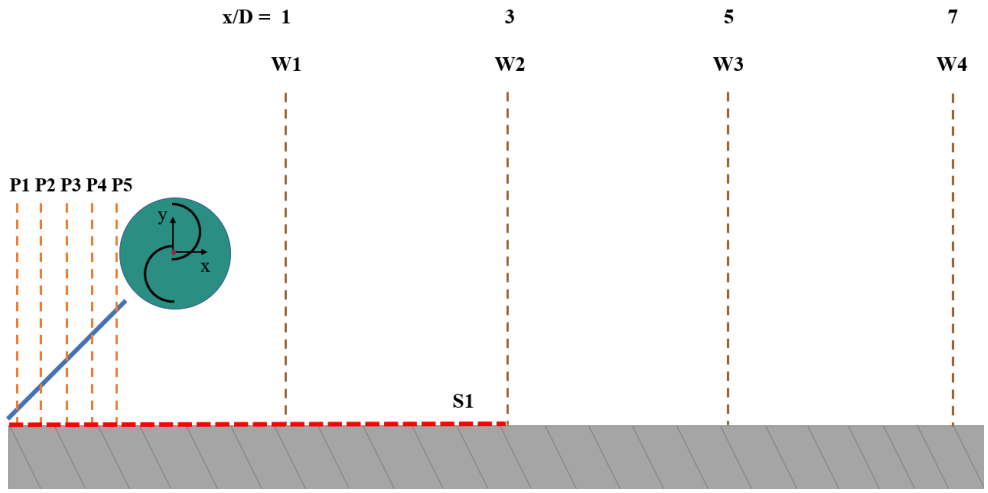

Fig. 16. Diagram of selected research locations.

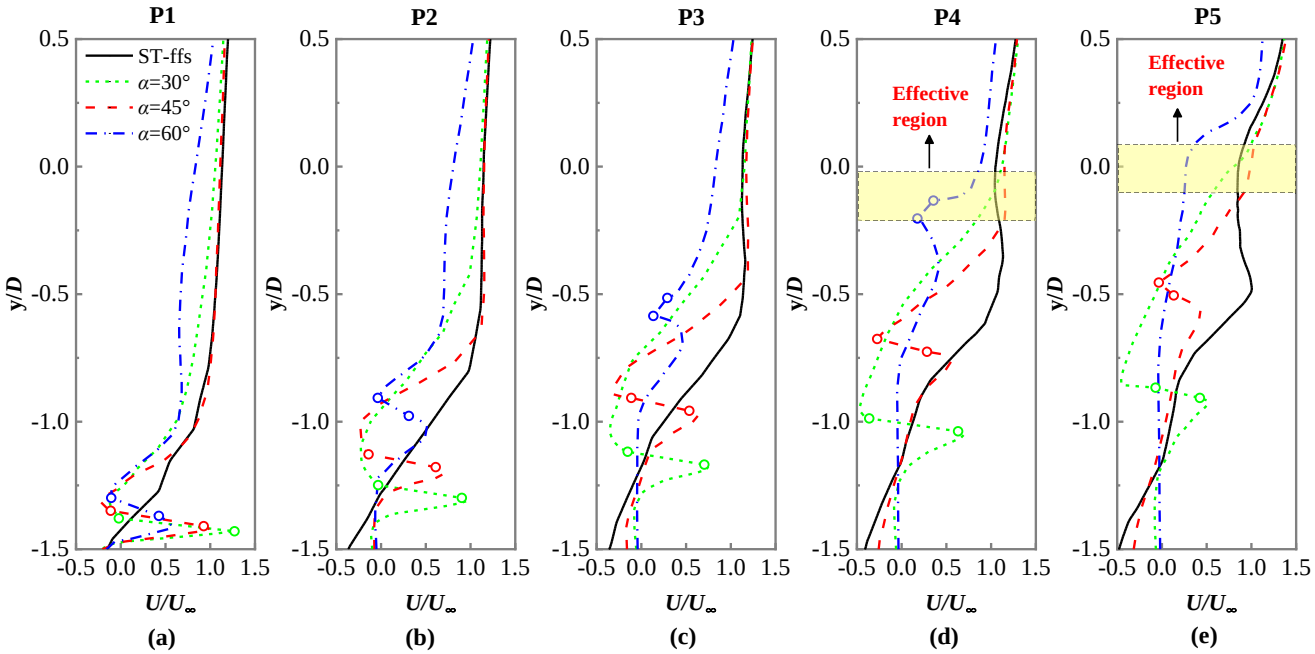

Fig. 17. Comparison of vertical profiles of normalised streamwise velocity at five isometric locations (dots indicate upper and lower surface boundaries of the panel, and $y/D = 0$ is the height of the turbine centre).

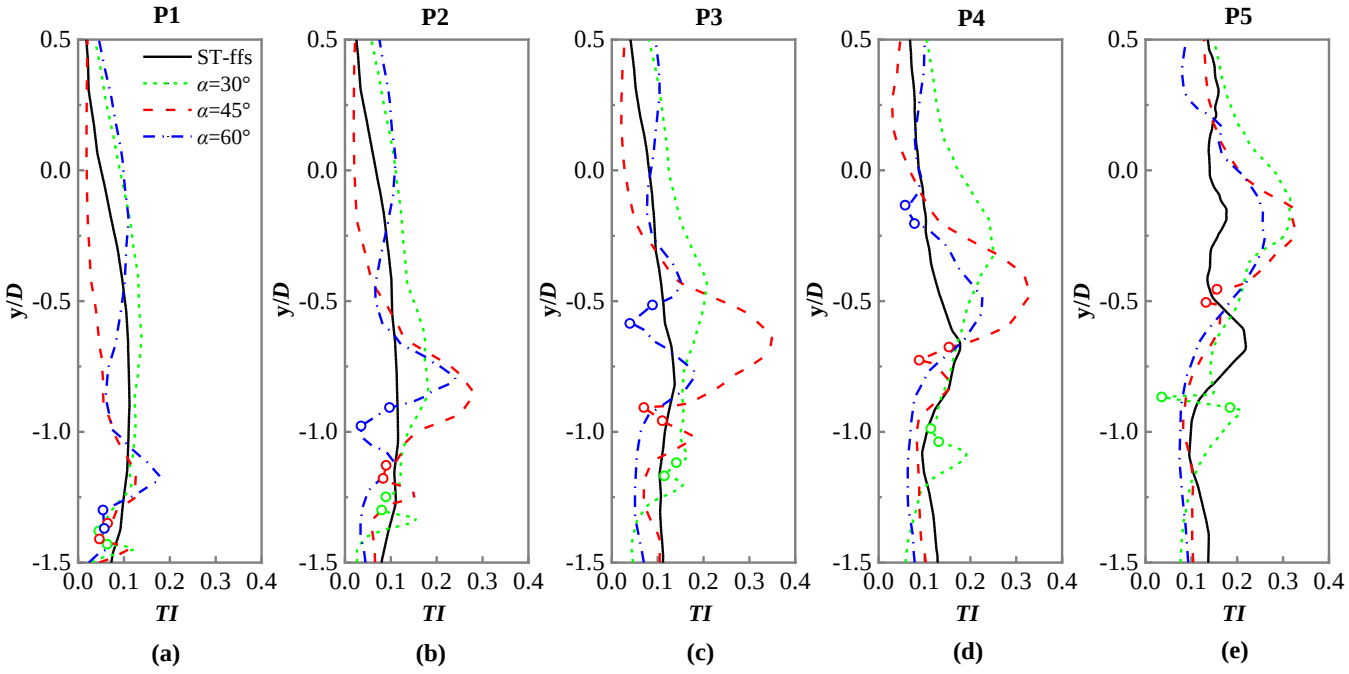

Fig. 18. Comparison of vertical profiles of turbulence intensity at five isometric locations (dots indicate upper and lower surface boundaries of the panel, and y/D = 0 is the height of the turbine centre).

Figs. 19 and 20 show a comparison of the vertical profiles of the normalised streamwise velocity and turbulence intensity for -1.5 < y/D < 1.5, respectively, at different positions (W1 to W4) in the wake region described in Fig. 16. The height of the Savonius turbine is indicated by the dotted yellow line. For W1 and W2, the normalised streamwise velocity and TI profile trends for the α = 60° case are different from the other cases because an excessive solar panel tilt angle significantly changes the flow field. It is also observed that the normalised streamwise velocity of the α = 60° case is lower at W1 and W2 in the wake region than in the other cases. The minimum velocity in the wake region occurs at approximately the height of the lower edge of the Savonius turbine, y/D = -1.5. In addition, observing the figure from left to right, as the wake develops, the normalised velocity in the region decreases, whereas the TI generally increases (especially at a height above the turbine, y/D > 0.5).

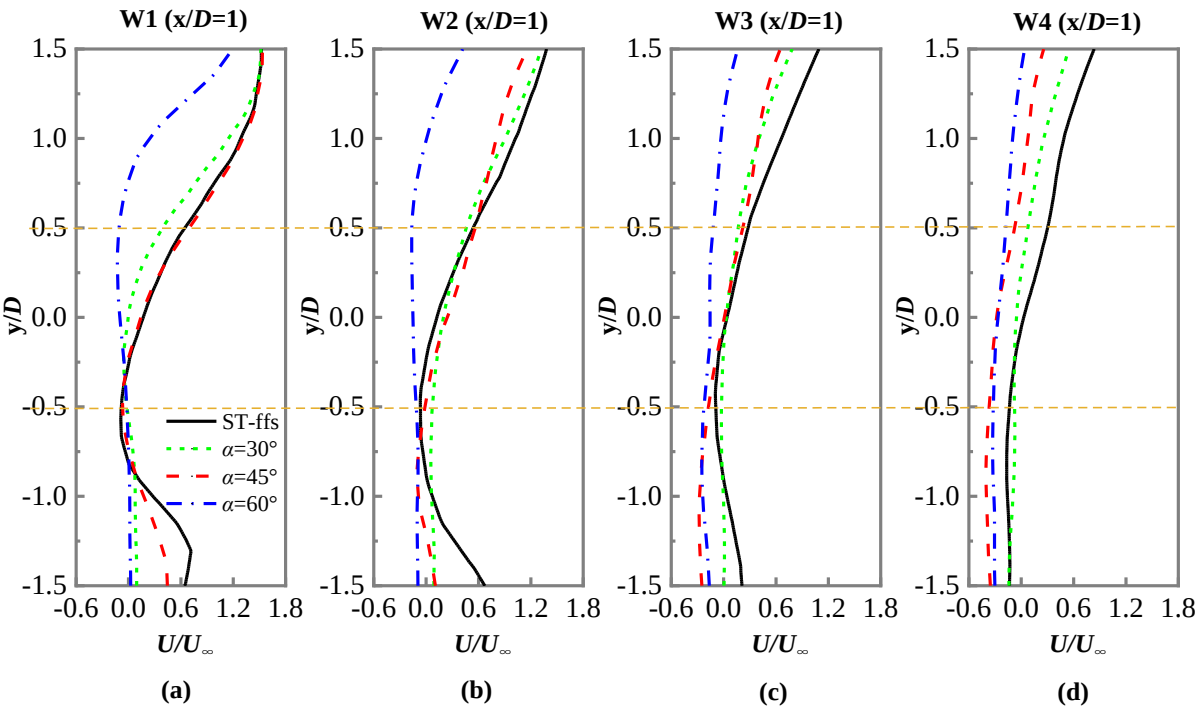

Fig. 19. Comparison of vertical profiles of normalised streamwise velocity in the wake region (the yellow dotted line indicates the height of the Savonius turbine).

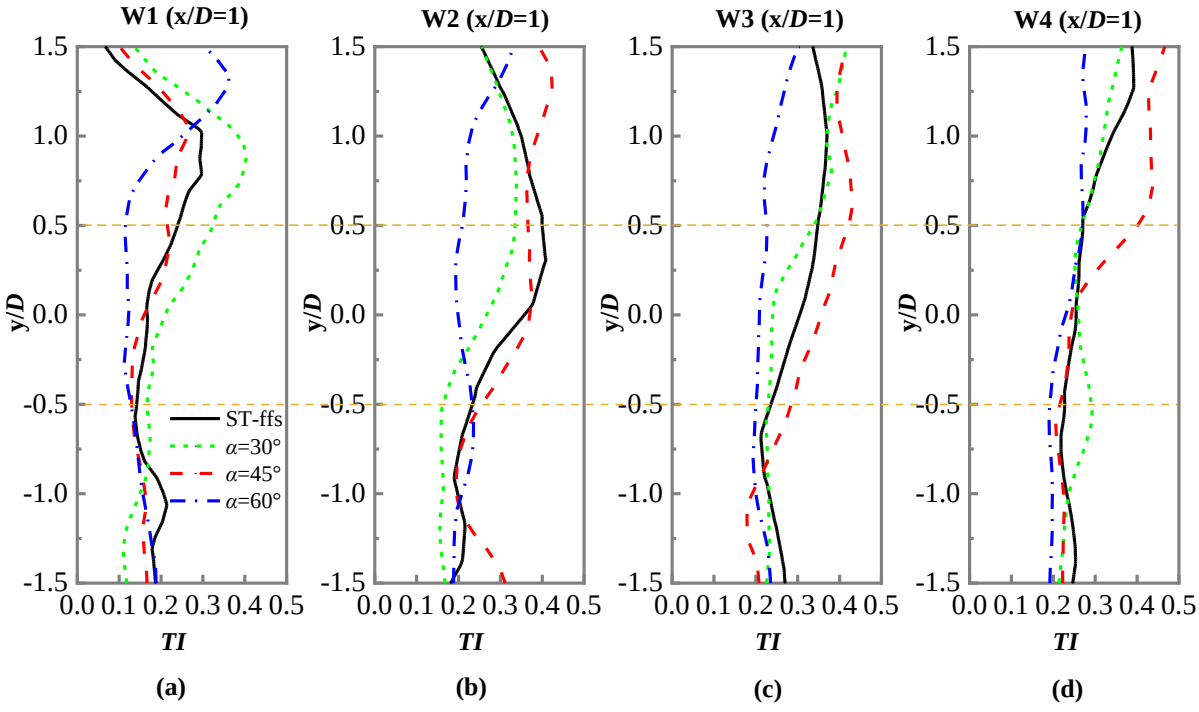

Fig. 20. Comparison of vertical profiles of turbulence intensity in the wake region (the yellow dotted line indicates the height of the Savonius turbine).

Fig. 21 illustrates a comparison of the horizontal profiles of the time-averaged normalized pressure for

the step surface location (S1) depicted in Figure 16. The location of the Savonius turbine is indicated by the yellow area. It can be seen that in the wind-solar energy hybrid harvesting system, the negative wind pressure on the step surface shows smaller magnitudes than that in the case of only a forward-facing step. That is, the Savonius wind turbine and solar panel placed on the step reduce the wind suction on the step surface. Therefore, in the novel system proposed in this study, the effect of reducing the wind load on the step surface can be achieved.

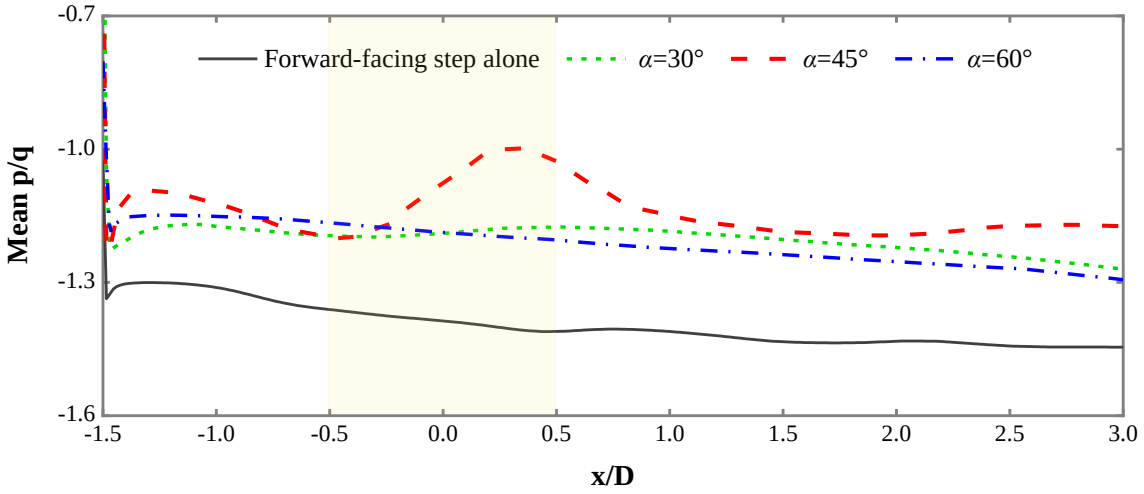

Fig. 21. Comparison of horizontal profiles of time-averaged normalized pressure on the step surface (yellow area indicates the location of the Savonius turbine).

4.3. Estimation of Carbon Dioxide emission reductions

Fig. 21 gives a brief quantitative estimation of the CO_2 emission reductions that can be achieved from a Savonius wind turbine. In this study, the highest power coefficient of the Savonius wind turbine reaches 0.638, and the corresponding power output is 0.25 kW. Based on the 35% capacity factor[45], it is assumed that the actual load hours per day for a Savonius wind turbine are 8.0 h, namely, the ratio between the actual load hours per year (2920 h are assumed) and the maximum number of hours in a year (8760 h) is 33.33%. The electricity loss in the system was assumed to be negligible[46], and the annual power generation of a Savonius wind turbine is 730 kWh. According to the China Power Industry Annual Development Report 2021, the national

CO_2 emissions per unit of thermal power generation are about 832 g/kWh[47]. Thus, the annual CO_2 emission reduction of a Savonius wind turbine in the novel hybrid system (ST-ffs-sp) reaches 606 kg. Under the same conditions, compared with a Savonius wind turbine placed on the building roof (ST-ffs) and a Savonius wind turbine alone (ST), the annual CO2 emission reduction for ST-ffs-sp is increased by 64 kg and 435 kg respectively.

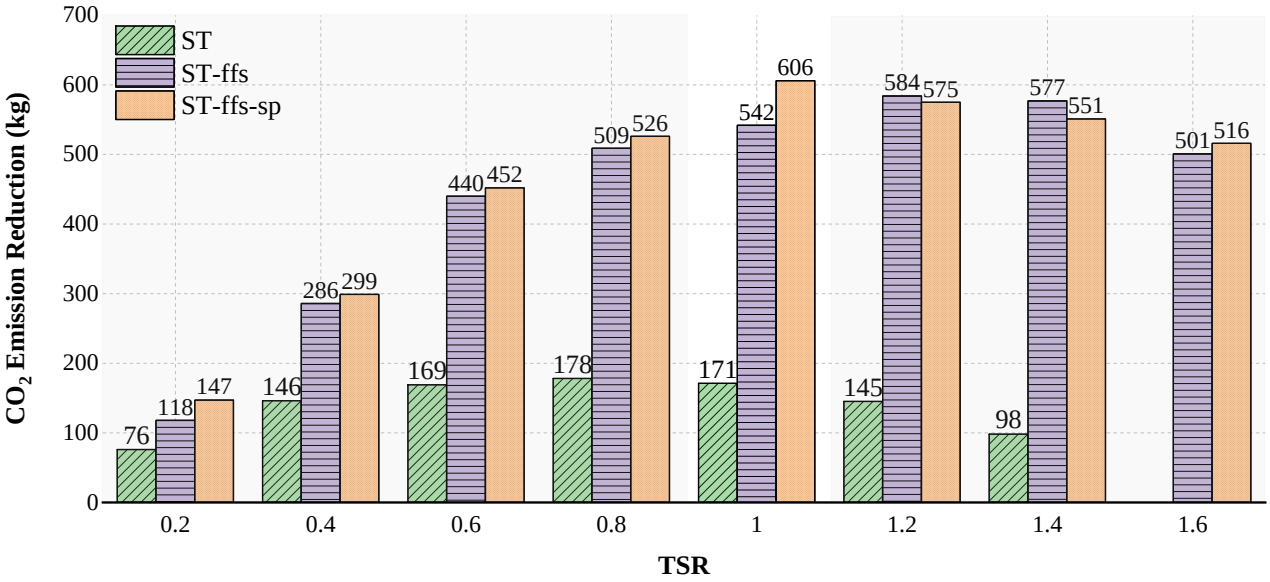

Fig. 21. Comparison of CO2 emission reductions from a Savonius wind turbine for wind power generation at different TSRs.

5. Conclusion and future perspectives

In this study, a wind-solar energy hybrid harvesting system combining an inclined solar panel and a Savonius wind turbine installed on a building roof was proposed for more stable power generation and improved energy utilisation. High-fidelity numerical simulations (LES) were performed on a three-dimensional scaled model. At an incoming wind speed of 7 m/s, the effect of tilt angle on the aerodynamic performance of a Savonius wind turbine was investigated and compared to two base cases to determine the optimal tilt angle. Subsequent simulations were performed for multiple TSRs, and the relevant flow-field characteristics were analysed. The primary conclusions are summarised as follows.

(1) In the novel hybrid system, the aerodynamic performance of the Savonius wind turbine can be significantly improved. When the turbine is operating at a TSR of 1.0, the power coefficient of the Savonius turbine increased and then decreased with an increase in the tilt angle of the solar panel. The maximum power coefficient (C_{pmax} = 0.638) occurred at a tilt angle of approximately 45°. At this condition, C_{pmax} was 254.4% higher than the power coefficient of a Savonius turbine alone ($C_{p,\,ST}$ = 0.180) and 11.7% higher than the power coefficient of a Savonius turbine placed on a forward-facing step ($C_{p,\,ST\text{-}ffs}$ = 0.571).

(2) For different installation cases, the peak power coefficient was observed at different TSR values. It occurs at approximately TSR = 1.0 in the hybrid system with a tilt angle α = 45° (C_{pmax} = 0.638), at TSR = 0.8 for a wind turbine alone ($C_{p\,(max,\,ST)}$ = 0.187), and at TSR = 1.2 for a Savonius turbine placed on a forward-facing step ($C_{p\,(max,\,ST\text{-}ffs)}$ = 0.615). C_{pmax} was 241.2% greater than $C_{p\,(max,\,ST)}$ and 3.7% greater than $C_{p\,(max,\,ST\text{-}ffs)}$. In summary, the Savonius wind turbine in the hybrid system with a 45° tilt angle exhibits the most excellent wind energy conversion performance.

(3) The improved wind turbine performance results from the changes of flow field guided by the hybrid system. When a Savonius turbine is installed on a forward-facing step, an acceleration flow region is formed in front of the turbine owing to the Venturi effect. By introducing a solar panel with a 45° tilt angle, part of the airflow that originally flowed to the passage near the returning blade is blocked, increasing the airflow speed in the acceleration region. The airflow with higher velocity hits the advancing blade, producing a larger pressure difference (mainly due to the decrease in the low pressure on the concave surface of the advancing blade), resulting in an increase in the net torque applied to the turbine blades and increasing the power coefficient of the Savonius turbine. When the tilt angle of the solar panel is too large (60°), the airflow is unable to directly hit the advancing blade due to unsuitable guidance, resulting in turbine failure. When the tilt angle of the solar panel is low (30°), the original acceleration region is destroyed, leading to a reduction in the power coefficient. Thus, a hybrid system with a suitable tilt angle can improve the aerodynamic

performance of the Savonius turbine and increase its energy collection efficiency.

Limitations to this study are also stated herein for the reference to further research. In this study, a canonical forward step model was applied to represent a flat roof building, which shows similar flow dynamics. In the real world, the shape of the building roof is much more complex, and the performance of the proposed hybrid system will be validated for real buildings. This system also contains many parameters that can be studied, such as the shape and tilt angle of the solar panel, the tip speed ratio, overlap ratio, aspect ratio and blade shape of the Savonius wind turbine [48, 49]. However, due to the limitations of the length and structure of the article, two of the most important parameters are discussed in this paper, namely the tilt angle and the tip speed ratio. Future work will include the investigation and optimization of other parameters in this hybrid system and even the extension of the research to the field of hydrokinetic turbines [50]. In addition, this study mainly focuses on the aerodynamic performance of the wind turbine in the proposed hybrid system, and the solar energy harvesting efficiency of the solar panel will also be explored in future work [51].

Acknowledgements

The support for this work by the National Natural Science Foundation of China (Grant No. 51908107) is gratefully acknowledged.

References

[1] D. Mauree, E. Naboni, S. Coccolo, A.T.D. Perera, V.M. Nik, J.-L. Scartezzini, A review of assessment methods for the urban environment and its energy sustainability to guarantee climate adaptation of future cities, Renewable and Sustainable Energy Reviews 112 (2019) 733-746.

[2] M. Mahmoud, M. Ramadan, A.-G. Olabi, K. Pullen, S. Naher, A review of mechanical energy storage systems combined with wind and solar applications, Energy Conversion and Management 210 (2020) 112670.

[3] L. Zeng, F. Zhao, H. Wang, Z. Wang, W. Yeung, Y. Liu, H.J.A.P.L. Tang, A bi-directional flow-energy harvester, 122(15) (2023) 153901.

[4] F.W. Zhao, Q. Jiang, Z.K. Wang, M.N.M. Qadri, L. Li, H. Tang, Interaction of two fully passive flapping foils arranged in tandem and its influence on flow energy harvesting, ENERGY 268 (2023).

[5] M.N. Mumtaz Qadri, F. Zhao, H. Tang, Fluid-structure interaction of a fully passive flapping foil for flow energy

extraction, International Journal of Mechanical Sciences 177 (2020) 105587.
[6] E. Pinheiro, F. Bandeiras, M. Gomes, P. Coelho, J. Fernandes, Performance analysis of wind generators and PV systems in industrial small-scale applications, Renewable and Sustainable Energy Reviews 110 (2019) 392-401.
[7] Q. Huang, Y. Shi, Y. Wang, L. Lu, Y. Cui, Multi-turbine wind-solar hybrid system, Renewable Energy 76 (2015) 401-407.
[8] L.-q. Liu, Z.-x. Wang, The development and application practice of wind–solar energy hybrid generation systems in China, Renewable and Sustainable Energy Reviews 13(6) (2009) 1504-1512.
[9] J.Y. He, P.W. Chan, Q.S. Li, C.W. Lee, Characterizing coastal wind energy resources based on sodar and microwave radiometer observations, RENEWABLE & SUSTAINABLE ENERGY REVIEWS 163 (2022).
[10] P. Škvorc, H. Kozmar, Wind energy harnessing on tall buildings in urban environments, Renewable and Sustainable Energy Reviews 152 (2021) 111662.
[11] F. Toja-Silva, T. Kono, C. Peralta, O. Lopez-Garcia, J. Chen, A review of computational fluid dynamics (CFD) simulations of the wind flow around buildings for urban wind energy exploitation, J. Wind. Eng. Ind. Aerodyn. 180 (2018) 66-87.
[12] J. Wen, L. Zhou, H. Zhang, Mode interpretation of blade number effects on wake dynamics of small-scale horizontal axis wind turbine, Energy 263 (2023) 125692.
[13] H. Zhang, J. Wen, J. Zhan, D. Xin, Effects of blade number on the aerodynamic performance and wake characteristics of a small horizontal-axis wind turbine, Energy Conversion and Management 273 (2022) 116410.
[14] R. Howell, N. Qin, J. Edwards, N. Durrani, Wind tunnel and numerical study of a small vertical axis wind turbine, Renewable Energy 35(2) (2010) 412-422.
[15] M. Hassanpour, L.N. Azadani, Aerodynamic optimization of the configuration of a pair of vertical axis wind turbines, Energy Conversion and Management 238 (2021) 114069.
[16] R. Kumar, K. Raahemifar, A.S. Fung, A critical review of vertical axis wind turbines for urban applications Renewable and Sustainable Energy Reviews 89 (2018) 281-291.
[17] L. Ledo, P.B. Kosasih, P. Cooper, Roof mounting site analysis for micro-wind turbines, Renewable Energy 36(5) (2011) 1379-1391.
[18] S.C. Goh, J.U. Schlüter, Numerical simulation of a Savonius turbine above an infinite-width forward facing step, Wind Engineering 40(2) (2016) 134-147.
[19] X. Liu, D. Zhao, N.L. Oo, Numerical prediction of the power coefficient improvements of three laterally aligned Savonius wind turbines above a forward facing step, J. Wind. Eng. Ind. Aerodyn. 228 (2022).
[20] Larin.P., Paraschivoiu.M., Aygun.C., CFD based synergistic analysis of wind turbines for roof mounted integration, Journal of Wind Engineering Industrial Aerodynamics 156 (2016) 1-13.
[21] J.V. Akwa, H.A. Vielmo, A.P. Petry, A review on the performance of Savonius wind turbines, Renewable & Sustainable Energy Reviews 16(5) (2012) 3054-3064.
[22] J.P. Abraham, B.D. Plourde, G.S. Mowry, W.J. Minkowycz, E.M. Sparrow, Summary of Savonius wind turbine development and future applications for small-scale power generation, JOURNAL OF RENEWABLE AND SUSTAINABLE ENERGY 4(4) (2012).
[23] D. Zhao, N. Han, Optimizing overall energy harvesting performances of miniature Savonius-like wind harvesters, Energy Conversion and Management 178 (2018) 311-321.
[24] H.L. Bai, C.M. Chan, X.M. Zhu, K.M. Li, A numerical study on the performance of a Savonius-type vertical-axis wind turbine in a confined long channel, Renewable Energy 139 (2019) 102-109.
[25] R. Mereu, D. Federici, G. Ferrari, P. Schito, F. Inzoli, Parametric numerical study of Savonius wind turbine interaction in a linear array, Renewable Energy 113 (2017) 1320-1332.
[26] R. Patel, V. Patel, Performance analysis of Savonius hydrokinetic turbine using 'C' shaped Deflector, Energy Sources, Part A: Recovery, Utilization, and Environmental Effects 44(3) (2022) 6618-6631.
[27] V.K. Patel, R.S. Patel, Optimization of an angle between the deflector plates and its orientation to enhance the energy efficiency of Savonius hydrokinetic turbine for dual rotor configuration, International Journal of Green Energy 19(5)

(2022) 476-489.
[28] H. Aboujaoude, F. Beaumont, S. Murer, G. Polidori, F. Bogard, Aerodynamic performance enhancement of a Savonius wind turbine using an axisymmetric deflector, J. Wind. Eng. Ind. Aerodyn. 220 (2022).
[29] P.K. Talukdar, N. Alom, U.H. Rathod, V. Kulkarni, Alternative Blade Profile Based on Savonius Concept for Effective Wind Energy Harvesting, Journal of Energy Resources Technology-Transactions of the Asme 144(4) (2022).
[30] M.H. Mohamed, G. Janiga, E. Pap, D. Thevenin, Optimal blade shape of a modified Savonius turbine using an obstacle shielding the returning blade, Energy Conversion and Management 52(1) (2011) 236-242.
[31] K. Golecha, T.I. Eldho, S.V. Prabhu, Influence of the deflector plate on the performance of modified Savonius water turbine, Applied Energy 88(9) (2011) 3207-3217.
[32] K.H. Wong, W.T. Chong, N.L. Sukiman, S.C. Poh, Y.-C. Shiah, C.-T. Wang, Performance enhancements on vertical axis wind turbines using flow augmentation systems: A review, Renewable and Sustainable Energy Reviews 73 (2017) 904-921.
[33] H.Y. Peng, S.S. Song, H.J. Liu, S.F. Dai, F.L. Zhang, Investigation of wind loading characteristics of roof-mounted solar panels on tall buildings, Sustainable Energy Technologies and Assessments 54 (2022) 102800.
[34] F. Toja-Silva, C. Peralta, O. Lopez-Garcia, J. Navarro, I. Cruz, Effect of roof-mounted solar panels on the wind energy exploitation on high-rise buildings, J. Wind. Eng. Ind. Aerodyn. 145 (2015) 123-138.
[35] N. Franchina, G. Persico, M. Savini, 2D-3D Computations of a Vertical Axis Wind Turbine Flow Field: Modeling Issues and Physical Interpretations, Renewable Energy 136 (2019) 1170-1189.
[36] G. Ferrari, D. Federici, P. Schito, F. Inzoli, R. Mereu, CFD study of Savonius wind turbine: 3D model validation and parametric analysis, Renewable Energy 105 (2017) 722-734.
[37] C. Li, S.Y. Zhu, Y.L. Xu, Y.Q. Xiao, 2.5D large eddy simulation of vertical axis wind turbine in consideration of high angle of attack flow, Renewable Energy 51 (2013) 317-330.
[38] N. Fujisawa, On the torque mechanism of Savonius rotors, J. Wind. Eng. Ind. Aerodyn. 40(3) (1992) 277-292.
[39] S.C. Goh, S.R. Boopathy, C. Krishnaswami, J.U. Schluter, Tow testing of Savonius wind turbine above a bluff body complemented by CFD simulation, Renewable Energy 87 (2016) 332-345.
[40] J.-O. Mo, A. Choudhry, M. Arjomandi, R. Kelso, Y.-H. Lee, Effects of wind speed changes on wake instability of a wind turbine in a virtual wind tunnel using large eddy simulation, J. Wind. Eng. Ind. Aerodyn. 117 (2013) 38-56.
[41] K.H. Wong, W.T. Chong, N.L. Sukiman, Y.C. Shiah, S.C. Poh, K. Sopian, W.C. Wang, Experimental and simulation investigation into the effects of a flat plate deflector on vertical axis wind turbine, Energy Conversion and Management 160 (2018) 109-125.
[42] I. Dobreva., F. Massouh, Cfd and piv investigation of unsteady flow through savonius wind turbine, Energy Procedia 6 (2011) 711-720.
[43] R. Longo, P. Nicastro, M. Natalini, P. Schito, R. Mereu, A. Parente, Impact of urban environment on Savonius wind turbine performance: A numerical perspective, Renewable Energy 156 (2020) 407-422.
[44] I. Abohela, N. Hamza, S. Dudek, Effect of roof shape, wind direction, building height and urban configuration on the energy yield and positioning of roof mounted wind turbines, Renewable Energy 50 (2013) 1106-1118.
[45] K.B. Oebels, S. Pacca, Life cycle assessment of an onshore wind farm located at the northeastern coast of Brazil, Renewable Energy 53 (2013) 60-70.
[46] M.S. Uddin, S. Kumar, Energy, emissions and environmental impact analysis of wind turbine using life cycle assessment technique, Journal of Cleaner Production 69 (2014) 153-164.
[47] X. Liu, X. Tao, Y. Wen, Y. Zeng, Improving carbon emission performance of thermal power plants in China: An environmental benchmark selection approach, Computers & Industrial Engineering 169 (2022) 108249.
[48] V. Patel, G. Bhat, T.I. Eldho, S.V. Prabhu, Influence of overlap ratio and aspect ratio on the performance of Savonius hydrokinetic turbine, International Journal of Energy Research 41(6) (2017) 829-844.
[49] R. Patel, V. Patel, Effect of waves on leading edge of modified Savonius rotor blades, Ocean Engineering 271 (2023) 113445.
[50] V. Patel, T.I. Eldho, S.V. Prabhu, Theoretical study on the prediction of the hydrodynamic performance of a Savonius

turbine based on stagnation pressure and impulse momentum principle, Energy Conversion and Management 168 (2018) 545-563.

[51] E. Biyik, M. Araz, A. Hepbasli, M. Shahrestani, R. Yao, L. Shao, E. Essah, A.C. Oliveira, T. del Caño, E. Rico, J.L. Lechón, L. Andrade, A. Mendes, Y.B. Atlı, A key review of building integrated photovoltaic (BIPV) systems, Engineering Science and Technology, an International Journal 20(3) (2017) 833-858.